Biological and Medical Applications of Materials and Interfaces

Label-Free Bimetallic In Situ Grown 3D Nickel Foam Supported NH2-MIL-88B(Fe2Co)-MOF based Impedimetric Immunosensor for the Detection of Cardiac Troponin I

Sathyadevi Palanisamy, Duraisamy Senthil Raja, Boopathi Subramani, Tung-Ho Wu, and Yun-Ming Wang

ACS Appl. Mater. Interfaces, **Just Accepted Manuscript** • DOI: 10.1021/acsami.0c09086 • Publication Date (Web): 24 Jun 2020

Label-Free Bimetallic In Situ Grown 3D Nickel Foam Supported NH_2-MIL-88B(Fe_2Co)-MOF based Impedimetric Immunosensor for the Detection of Cardiac Troponin I

Sathyadevi Palanisamy,[1] Duraisamy Senthil Raja,[2] Boopathi Subramani,[3] Tung-Ho Wu,[4] and Yun-Ming Wang[1,2,]*

[1]Department of Biological Science and Technology, Institute of Molecular Medicine and Bioengineering, Center for Intelligent Drug Systems and Smart Bio-devices(IDS^{2}B), National Chiao Tung University, Hsinchu 300, Taiwan.

[2]Department of Chemical Engineering, National Tsing Hua University, Hsinchu 300, Taiwan.

[3]Department of Food Safety/Hygiene and Risk Management, College of Medicine, National Cheng Kung University, Tainan 701, Taiwan.

[4]Division of Cardiovascular Surgery, Department of Surgery and Division of Surgical Critical Care, Department of Critical Care Medicine, Veterans General Hospital, Kaohsiung 813, Taiwan.

[5]Department of Biomedical Science and Environmental Biology, Center for Cancer Research, Kaohsiung Medical University, Kaohsiung 807, Taiwan.

*Corresponding author: Yun-Ming Wang: ymwang@mail.nctu.edu.tw

Keywords: metal-organic framework, nickel foam, immunosensor, biomarker, cardiac troponin I

ABSTRACT

In this study, a simple and competent metal-organic framework (MOF) based nickel foam (NF) supported 3D immunosensor (Ab-NH_2-MIL-88B(Fe_2Co)-MOF/NF) was constructed and utilized for the specific recognition of the biomarker cardiac troponin (I). In the present work, the biosensor fabrication was progressed through the modification of the NF substrate with MOF material (NH_2-MIL-88B(Fe_2Co)-MOF) to enable amine functionalized electrode. This amine functionalized NF electrodes (NH_2-MIL-88B(Fe_2Co)-MOF/NF) were then bio-interfaced with anti-cTnI antibodies and ended up as Ab-NH_2-MIL-88B(Fe_2Co)-MOF/NF electrodes. Analytical executions of the constructed bio-electrode were investigated for the quantitative analysis of cTnI in both buffered and serum solutions. Then, the electrochemical studies were carried out using the electrochemical impedance spectroscopy (EIS) method by monitoring changes concerning the charge transfer resistance (R_{ct}) characteristics. The limit of detection (LOD) of Ab-NH_2-MIL-88B(Fe_2Co)-MOF/NF immunosensor was achieved to be 13 fg/ml with great specificity. This kind of immunosensor imparts a new platform for the construction and application of MOF-hybrid 3D electrode materials with enhanced electrochemical behavior in cTnI sensing for the first time.

INTRODUCTION

Cardiovascular diseases (CVDs) including cerebrovascular disease, congenital heart disease, coronary heart disease, rheumatic heart disease, acute myocardial infarction, and peripheral arterial disease are contemplated as a major risk to global health.[1] This focus to design new reliable, accurate, and rapid point-of-care (POC) devices to detect CVD. The AMI diagnosis is carried out by examining various parameters including chest pain, diagnosing the changes in the electrocardiogram, and measuring the elevation of a crucial cardiac biomarker in the blood samples.[2] Cardiac troponins (cTn), myoglobin, creatine kinase isoforms, and creatine phosphokinase are the potential cardiac biomarkers that are available for the AMI diagnosis.[3] Among these biomarkers, cTnI behaves as a benchmark in AMI evaluation because of its high degree of specificity and sensitivity.[4] During the cardiac damage, the cTnI is discharged into the bloodstream within 12 h and the level reached between 0.7-1.4 ng/ml starting from the normal level of <0.4 ng/ml and stays upraised till 5-9 days.[5] Since early AMI diagnosis is a crucial need, the levels of cTnI should be tested immediately within few hours after suspecting the onset of AMI. Various limitations are filed against the existing conventional methods such as field-effect transistor-based analysis,[6] electrochemiluminescence,[7] fluorescence,[8] and enzyme linked immunosorbent assay,[9] etc. The limitations are low sensitivity, high-cost instrumentations, and time taking experimental processes. Therefore, a highly sensitive detection technique is required to achieve an early diagnosis of AMI.

Electrochemical sensors are powerful and contribute to real time detection. Sensors developed using this methodology are very easy to handle since it acts like a miniaturized POC devices. Potentiometric, impedimetric, and conductance-based sensors operate under the electrochemical principle. Out of these methodologies, the outcome of immunosensor based on

EIS detection can provide an accurate, rapid, direct and selective method for biological samples.[10-15] Impedimetric sensors record the impedance changes of the newly fabricated impedimetric sensors that were recorded by supplying the potential to the electrode. With the availability of an electrolyte, polarization occurs and the charges migrate towards the electrode surface and build an electric double layer. The pocket charges undergo modulations during the protein-antibody interactions on the electrode surface.

MOFs are a class of well-ordered crystalline coordination polymers possessing many attractive characteristics and potential applications in various fields including materials, biological, energy, and environmental areas.[16-21] MOFs have a huge amount of metallic ions, yielding high electrochemical signals while undergoing electrochemical detection. MOFs and MOFs-derived hybrid materials are well known for their electrochemical applications[22-24] owing to its permanent porous structure, presence of uniform conductive carbon scaffold, and ultra-small active materials. This type of construction further enables MOFs to serve as a potential candidate for self-supported electrodes.[25] In recent days, MOFs are being used as electrode materials which are important in biochemistry for developing high sensitive electrochemical methods for potential detection of trace amount of biological compounds. The superior properties of MOFs including incredible high surface area various pore sizes, availability of active sites, and controlled surface properties enable them ideal biosensor for electrochemical reactions.[26-27]

The NF is a 3D mesoporous substrate acting as a support for conducting electrocatalytic studies. It is known for its promising characteristics such as high electrical conductance, flexibility, high mechanical strength, and comparatively high surface areas as compared with other available supports.[28-29] The MOFs have been hard being studied as electroactive materials since it possesses low electrical conductivities. The presence of macroporous channels (pore size of several hundred

micrometers) in NF can provide increased mass transfer associated with electrochemical processes.[30] In particular, in situ growth of nanosized MOFs over NF backbones efficiently improves the charge carrier transport and greatly enhances overall charge transfer of the electrode. The poor water stability of electro-active MOFs restricts their practice in the field of electrochemical detection since most of the reactions are performed in aqueous solutions.[31] Hence, in this study, an electro-conducting bimetallic in situ grown MOF on NF was constructed with a formula of Fe_2Co-MOF/NF to work in the aqueous conditions. This study utilizing the in situ grown MOF on NF is the first report to demonstrate the use of such material directly as an electrochemical immunosensor for the recognition of cTnI biomarkers.

In the current study, the design and hydrothermal synthesis of a new class of in situ grown bimetallic MOF supported on NF (NH_2-MIL-88B(Fe_2Co)-MOF/NF) materials were reported for the immunosensing of cTnI. The NH_2-MIL-88B(Fe_2Co)-MOF was derived from the Fe_2Co cluster ($[Fe_2CoO(CH_3COO)_6(H_2O)_3]\cdot 3H_2O$) and 2-amino terephthalic acid ($H_2BDC\text{-}NH_2$) using hydrothermal synthesis. The as-prepared NH_2-MIL-88B(Fe_2Co)-MOF/NF serves as a working electrode to carry out electrochemical performances. The surface morphologies and the electrochemical characteristics were studied before and after surface modification with antibodies. The fabricated electrode is now suitable to detect the various concentrations of target analytes, cTnI. The different processes associated with the immunosensor fabrication, surface modification of immunosensor with antibody, and antigen detection were mainly studied using electrochemical techniques such as EIS and cyclic voltammetry (CV). This type of immunosensor provided a new floor for the fabrication and practical use of 3D MOF-hybrid electrode materials with enhanced electrochemical behavior in cTnI sensing for the first time.

EXPERIMENTAL SECTION

Materials

Ferric nitrate nonahydrate $Fe(NO_3)_3$. $9H_2O$ and cobaltous nitrate $Co(NO_3)_2.6H_2O$, sodium acetate trihydrate ($CH_3COONa \cdot 3H_2O$), 2-aminoterephthalic acid ($H_2BDC\text{-}NH_2$), acetic acid, and dimethylformamide (DMF) were purchased from Alfa Aesar. Human cTnI (98%), human cardiac troponin T, cTnT (98%), avidin, follicle stimulating hormone (FSH), 1-ethyl-3-(3-dimethyl amino propyl) carbodiimide (EDC), N-hydroxy succinimide (NHS), potassium ferrocyanide ($K_4[Fe(CN)_6$), potassium ferricyanide ($K_3[Fe(CN)_6]$ were purchased from Sigma Aldrich company (MO, USA). The nickel foams were commercially purchased from Changsha Liyuan Port (Changsha China). All other reagents and solutions used in this study were of high analytical grade and used without any further changes unless it is mentioned.

Methods

The electrochemical analyses EIS and CV were measured using an electrochemical analyzer, CH16275D with three electrodes set up. The morphology of the synthesized MOFs was recorded using Hitachi S-4800 Scanning Electron Microscopy (SEM), Japan. The Transmission Electron Microscopy (TEM) data were recorded using JEOL, JEM-2010 Instruments, Japan. The analysis of the composition of MOFs was done with the help of Oxford 6587 Energy Dispersive X-ray Spectroscopy (EDX), Oxford Instruments. Analysis of high phase purity and crystalline nature of the synthesized materials were determined using Shimadzu XRD-6000 Powder X-ray Diffractometer (PXRD), Japan. The measurements of X-ray Photoelectron Spectroscopic (XPS) details were performed to identify the elemental compositions of the synthesized materials in the presence of an excitation source, monochromatized Al Kα X-ray using Thermo ESCALAB 250XI, USA. The Brunauer-Emmett-Teller (BET) model depends on N_2 adsorption and desorption isotherm curves were determined for the synthesized NH_2-MIL-88B(Fe_2Co)-MOF materials to

find out their specific surface area using Micromeritics ASAP 2010 instruments. With the aid of Non-Local Density Functional Theory (NL-DFT), the pore size distribution of the materials was calculated. Fourier-Transform Infrared (FT-IR) spectroscopic data were obtained from the instrument JASCO FTIR-460 spectrophotometer in a frequency range of 400-4000 cm^{-1}. The samples were pelleted as potassium bromide (KBr) powders.

Synthesis

Synthesis of Fe_2Co mixed-metal cluster $[Fe_2CoO(CH_3COO)_6(H_2O)_3]\cdot 3H_2O$ (Fe_2Co cluster)

The Fe_2Co cluster was prepared using a similar method in the reported literature.[32-34] A 20 ml solution of $CH_3COONa.3H_2O$ (0.088 mol, 12 g) was added to a 20 ml filtered solution containing $Fe(NO_3)_3.9H_2O$ (0.0056 mol, 2.284 g) and $Co(NO_3)_2.6H_2O$ (0.028 mol, 8.308 g) and allowed for stirring about 24 h. After 24, the brown precipitate formed was filtered and then washed with a small quantity of water and ethanol alternatively three times. Finally, the product was dried in air.

Synthesis of NH_2-MIL-88B(Fe_2Co)-MOF/NF

The NH_2-MIL-88B(Fe_2Co)-MOF/NF was grown on NF support in one step by adapting the reported procedure with slight modifications.[35] Typically, a reaction mixture containing Fe_2Co-Cluster (400 mg), H_2BDC-NH_2 (350 mg), DMF (30 ml), acetic acid (1.5 ml), and one NF piece with a size of 2.5 cm x 2.5 cm was locked in a Teflon hydrothermal bomb. Then the stuffed Teflon bomb was kept inside an over for about 15 h maintaining at 150 ºC to obtain the insitu formation of NH_2-MIL-88B(Fe_2Co)-MOF over NF. After the reaction, an obvious color change was noticed for the MOF stacked NF. The NFs were collected and subjected for DMF and ethanol wash and finally dried at 70 ºC and stored for later use.

Immunosensor design and fabrication

An illustration of the design and fabrication of 3D impedimetric immunosensor is shown in **Scheme 1**. Before use, NFs were cut into pieces having a specific size of 2.5 × 2.5 cm and the sliced NFs were ultrasonicated with 3M hydrochloric acid for about 30 min to remove the deposited oxide layer present on their surfaces. Then the NFs washed alternatively with water and ethanol for three times and dried at 60 ºC in an oven. The Fe_2Co cluster was synthesized according to the reported method and was assembled on the surface of the cleaned NFs to produce Fe_2Co-MOF/NF based on the reported procedure with slight modifications. The as-produced NH_2-MIL-88B(Fe_2Co)-MOF/NF after biointerfacing with the cTnI antibody serves as a working electrode to execute the electrochemical processes. The antibody, antigen, and serum solutions freshly prepared using phosphate buffered solution (PBS), pH 7.4.

Biointerfacing of NH_2-MIL-88B(Fe_2Co)-MOF/NF electrode with cTnI antibody

To bioconjugate, the working area of the NH_2-MIL-88B(Fe_2Co)-MOF/NF electrodes with cTnI antibodies, freshly prepared solutions of EDC (200 mM, 50 µl) and NHS (50 mM, 50 µl) (1:1 v/v) were first incubated with cTnI antibody (0.1 mg/ml, 100 µl) solution for about 1 h at room temperature. The solutions were drop casted over the working areas of the constructed NH_2-MIL-88B(Fe_2Co)-MOF/NF electrode followed by incubation for another 1 h at 4 ºC. The cTnI antibody immobilization on the NH_2-MIL-88B(Fe_2Co)-MOF/NF electrode has occurred via amide bond formation. The resulted antibody (Ab) coated NH_2-MIL-88B(Fe_2Co)-MOF/NF (Ab-NH_2-MIL-88B(Fe_2Co)-MOF/NF electrode was rinsed with Tween 20 (0.01 %, pH 7.4) solution to remove any unbound biomolecules. To block the non-specific binding during target analysis, the Ab-NH_2-MIL-88B(Fe_2Co)-MOF/NF electrodes were incubated subsequently with bovine serum albumin (BSA)

(0.25 µg/ml, 50 µl) in PBS for 1 h. The biofunctionalized Ab-NH_2-MIL-88B(Fe_2Co)-MOF/NF electrodes were refrigerated at 4 ºC for later use.

Electrochemical Measurements

For the electrochemical measurements, cTnI antibody tagged Ab-NH_2-MIL-88B(Fe_2Co)-MOF/NF electrodes were used as a working electrode while Ag/AgCl electrodes were used as a reference electrode and a platinum wire as the auxiliary electrodes. An equimolar (10 mM) mixture containing $K_4[Fe(CN)_6]$ and $K_3[Fe(CN)_6]$ were employed as the redox probe to conduct all the EIS experiments. The electrochemical changes were recorded using $[Fe(CN)_6]^{3-/4-}$ as the redox couple. The EIS measurements were performed during different electrode construction stages including immunosensor fabrication, electrode biointerfacing with cTnI antibody, and cTnI antigen detection. The results were presented as Nyquist plots recorded in a frequency range (0.1 Hz – 0.1 MHz) at 0.5 mV sinusoidal voltage potential. The charge transfer resistance (R_{ct}) values were obtained from the EIS data upon fitting it in an equivalent circuit model. The CV studies were performed using $K_4[Fe(CN)_6]$ (10 mM) solution as an electrolyte maintaining a scan rate of 100 mV/s within a potential range of -1V - +1V.

Quantification of cTnI antigens

The analysis of cTnI detection was investigated in a concentration range of 1 ng/ml to 1 fg/ml. An aliquot of 10 µl of various cTnI antigen concentrations was exposed to antibody tagged Ab-NH_2-MIL-88B(Fe_2Co)-MOF/NF electrode working areas. It was then incubated for 10 min to assure the interactions between cTnI antibody-cTnI antigen. The electrodes were then washed with PBS and dried under nitrogen atmosphere before keeping it in an electrolytic solution for the electrochemical assessment. The applied potential for this study is in the range of -1 to +1 V.

Baselines were corrected by performing the blank analysis. The LOD of the designed immunosensor was calculated with the help of following equation:[36] LOD = 3.3 × S.D/s, where "S.D" is the standard deviation of the blank sample and "s" is the slope obtained from the calibration curve. The specificity of the functionalized immunosensor was analyzed by investigating the electrochemical response of Ab-NH_2-MIL-88B(Fe_2Co)-MOF/NF electrodes against a non-specific protein, FSH, avidin, and cTnT.

RESULTS AND DISCUSSION

The schematic of the label-free bimetallic in situ grown 3D NF supported NH_2-MIL-88B(Fe_2Co)-MOF based impedimetric immunosensor for cTnI antigen detection is presented in **Scheme 1.** As written in the experimental section, The NH_2-MIL-88B(Fe_2Co)-MOF/NF was synthesized in one step hydrothermal methods from the Fe_2Co cluster, H_2BDC-NH_2, and NF as starting materials (**Scheme 1**). The formation of NH_2-MIL-88B(Fe_2Co)-MOF on NF support is entirely uniform as one can observe from the color change of the material. This yielded high-quality NH_2-MIL-88B(Fe_2Co)-MOF/NF materials were judged from several characterization techniques. The structural and morphological behavior were investigated by the combination of various techniques including SEM, TEM, XPS, BET-Langmuir, DFT, PXRD, and FT-IR. To test the formation of nanostructure of the NH_2-MIL-88B(Fe_2Co)-MOF material coated on NF, some amount of NH_2-MIL-88B(Fe_2Co)-MOF was scratched off from NH_2-MIL-88B-(Fe_2Co)-MOF-NF and studied.

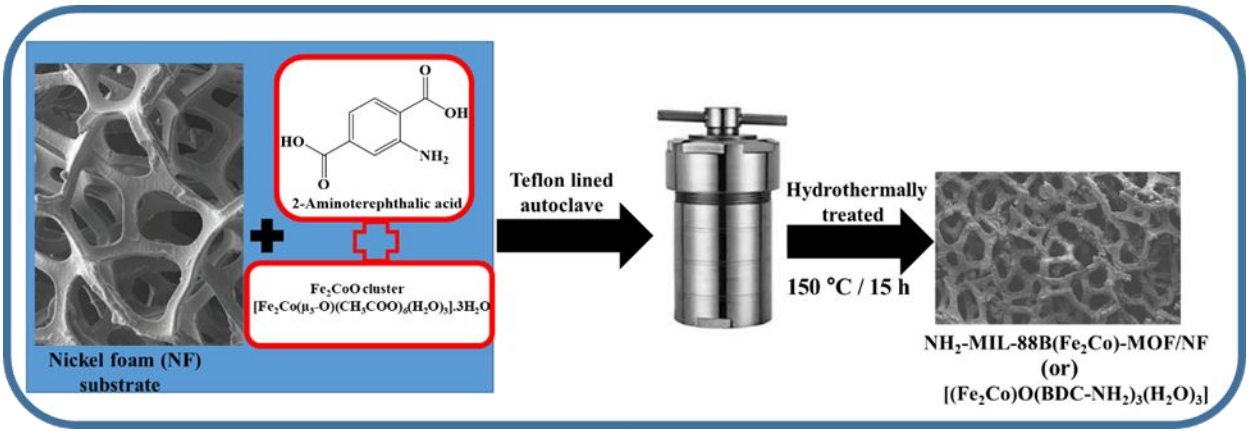

Scheme 1. An illustration of the in situ hydrothermal syntheses of NH_2-MIL-88B(Fe_2Co)-MOF nanospheres on NF derived from Fe_2Co-cluster, H_2BDC-NH_2 ligand, and NF piece at 150 ºC for 15 h resulting uniformly grown NH_2-MIL-88B(Fe_2Co)-MOF over the surface of NF.

The image obtained from SEM analysis showed that the NH_2-MIL-88B(Fe_2Co)-MOF particles grown on NF possesses nanosphere structures having an average particle size of 200 nm **(Figure 1a-g).** The EDX analysis of the NH_2-MIL-88B(Fe_2Co)-MOF revealed that the presence of main constituent elements such as carbon (C), oxygen (O), nitrogen (N), iron (Fe), and cobalt (Co) **(Figure S1).**

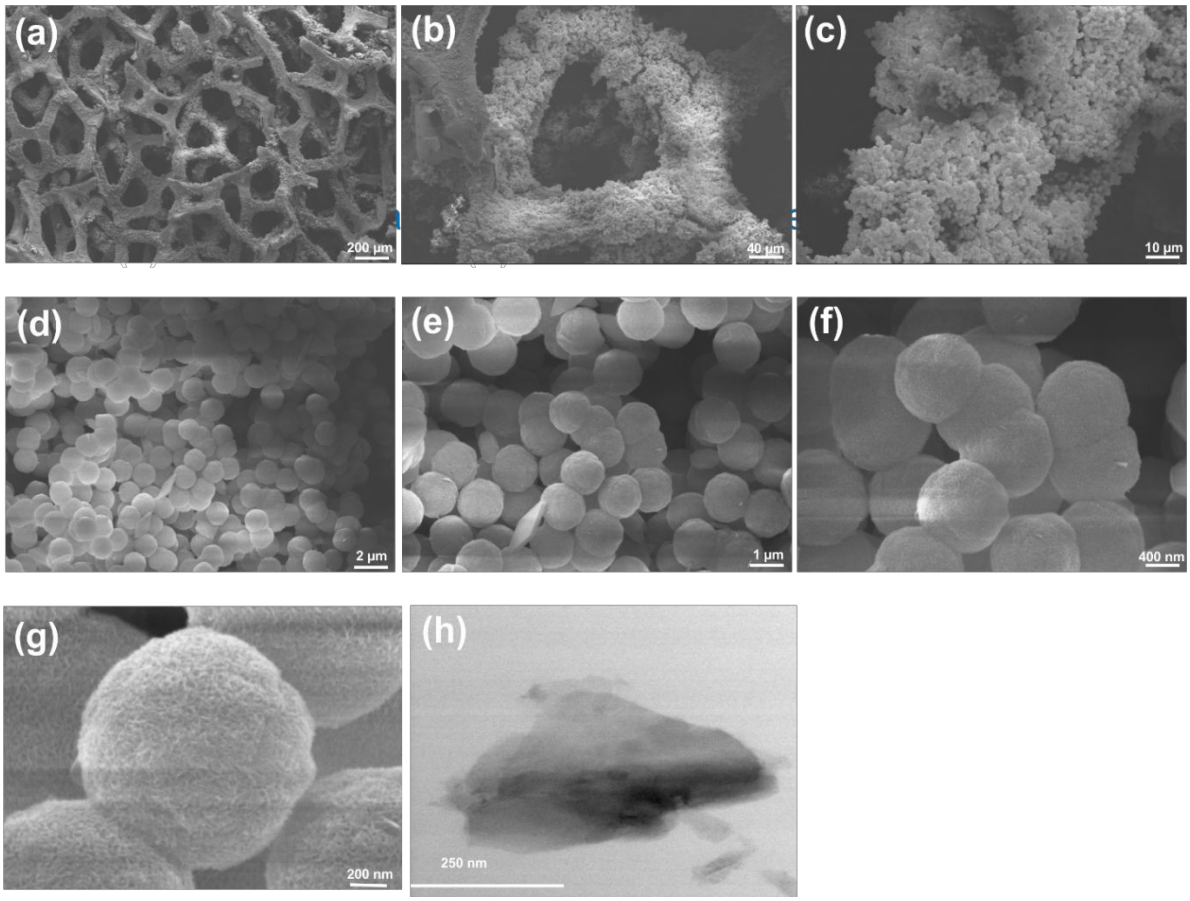

Figure 1. (a-g) SEM images of NH_2-MIL-88B(Fe_2Co) grown on NF. (h) TEM image of NH_2-MIL-88B(Fe_2Co) grown on NF.

The elemental analysis pattern of EDX analysis concluded that NH_2-MIL-88B(Fe_2Co)-MOF shares the same elemental composition. The comparison of atomic % values obtained from EDX analysis is in good agreement with the theoretically calculated values of NH_2-MIL-88B(Fe_2Co)-MOF. The image of area EDX elemental mapping for NH_2-MIL-88B(Fe_2Co)-MOF are shown in **Figure S2.** The TEM-EDX **(Figure 1 h)** of NH_2-MIL-88B(Fe_2Co)-MOF and its corresponding elemental mapping data **(Figure S3)** confirms the presence of all the constituent elements C, N, O, Fe, and Co, and the uniform distributions of these elements over the compound.

The crystalline structure of NH_2-MIL-88B(Fe_2Co) grown on NF was characterized with PXRD and the structure is identical with the simulated PXRD diffraction pattern of NH_2-MIL-88B(Fe_3) (**Figure 2a**). To investigate the electronic structure of the synthesized MOF, the XPS measurements were recorded for the scratched off NH_2-MIL-88B(Fe_2Co) from NF. The analysis of the XPS spectrum of the NH_2-MIL-88B(Fe_2Co) shows the presence of major constituent elements such as C, N, O, Fe, and Co (**Figure 2b**).

Furthermore, the HR-XPS spectrum of Fe2p (Figure 2c) can be de-convoluted to display binding energy peaks for $Fe2p_{3/2}$ and $Fe2p_{1/2}$ at 711.6 and 724.8 eV, respectively. The associated satellite peak was found at 717.6 eV. Also, the position of the peaks and the binding energy difference of 13.2 eV confirms the iron metal is present in the +3 oxidation sate in the MOF[37] whereas, the HR-XPS spectra of Co2p **(Figure 2d)** exhibits two major peaks for $Co2p_{3/2}$ and $Co2p_{1/2}$ at 780.5 and 795.5 eV, respectively. The corresponding two satellite peaks were observed at 785.2 and 803.2 eV, indicating the existence of cobalt metal in +2 oxidation state in the MOF.[38] The atomic ratio of Fe:Co obtained from the XPS results is close to 2:1 which is well agreed with the theoretically calculated values depending on the composition of MOF **(Figure 2e).**[33]

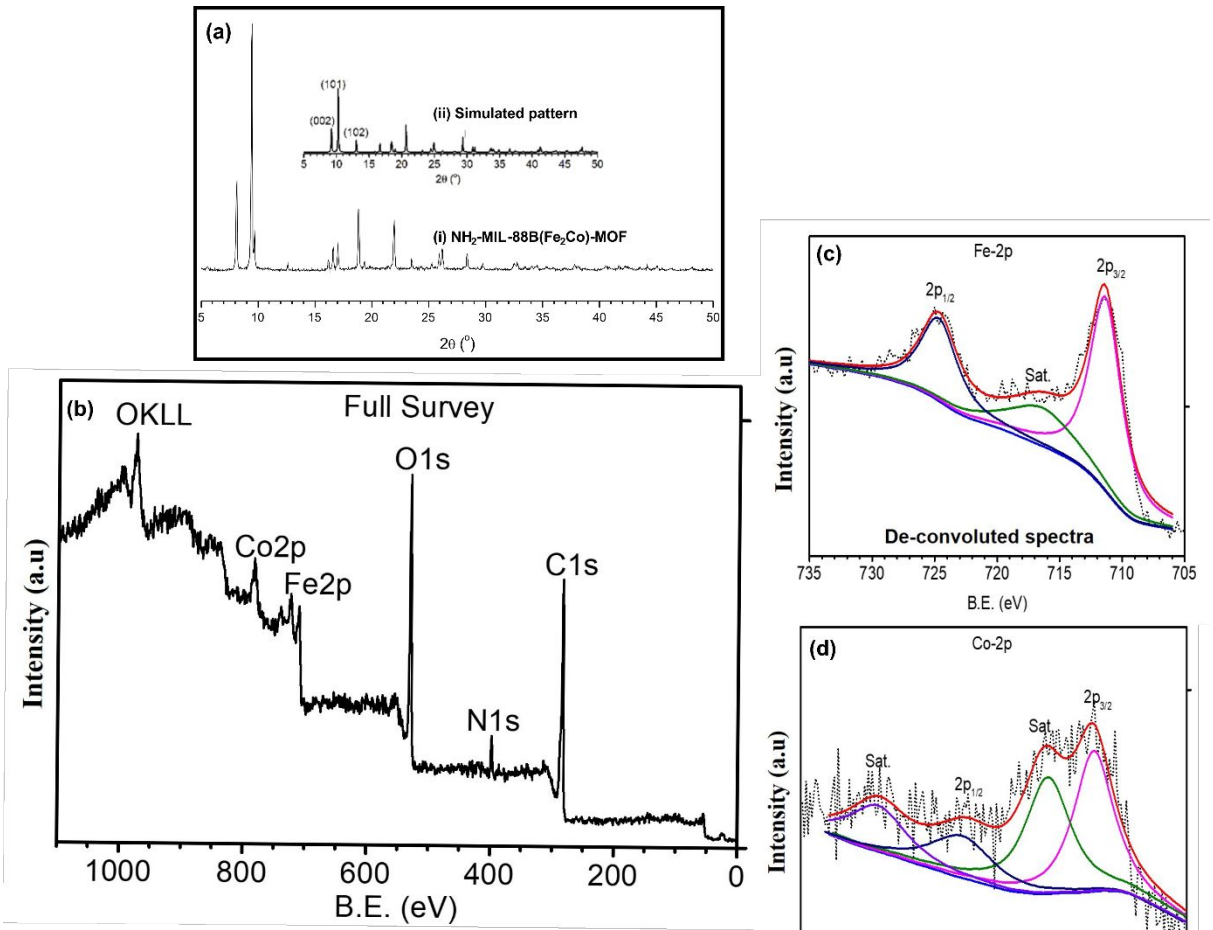

(e)

	C	O	N	Fe	Co	Fe:Co
Experimental	53.8	33.6	5.9	4.6	2.1	2.0:0.9
Calculated	52.2	34.8	6.5	4.3	2.2	2:1

Figure 2. (a) Images of (i) powder XRD patterns of NH_2-MIL-88B(Fe_2Co) and (ii) simulated pattern. (b) The XPS spectrum of scratched doff NH_2-MIL-88B(Fe_2Co) from NF showing the presence of major elements including C, N, O, Fe, and Co. (c, d) The high resolution XPS (HR-XPS) spectrum of Fe2p (de-convoluted spectra) and Co2p. (e) The elemental composition (atomic%) of the scratched off MOF, NH_2-MIL-88B(Fe_2Co) obtained from XPS results.

The porous characteristics of the scratched off MOF, NH_2-MIL-88B(Fe_2Co) was evaluated with N_2 gas sorption measurements recorded at 77 K. The N_2 gas sorption isotherms exhibit Type-I characteristics isotherm for microporous material, the rapid sorption pickup at low pressure indicates the microporous nature **(Figure 3a)**. The calculated specific surface areas are 405 and 523 m^2g^{-1} based on the BET model and Langmuir model, respectively. The pore size distribution results of NH_2-MIL-88B(Fe_2Co) derived using the DFT method are shown in Figure 3b, indicated

the pore sizes of 1.1 and 1.4 nm, which further confirms its microscopic nature. It is noteworthy to mention that the experiments were conducted using dry powders of NH_2-MIL-88B(Fe_2Co) material to identify the porous characteristics. An increase in the surface area and pore size of NH_2-MIL-88B(Fe_2Co)-MOF was noted when immersed the material in solvents like water which may be due to the breathing nature of MIL-88B type MOF materials [39] and this nature would be useful in biosensor applications.

In the FT-IR spectra **(Figure S4),** the Fe_2Co clusters show their characteristics peaks around 1400-1500 cm^{-1} which represents the stretching vibrations (symmetric and asymmetric) of the carboxylate group. The peak found at 3000 cm^{-1} indicates the presence of N-H stretching vibrations. The characteristic peak at ~600 cm^{-1} confirms the formation of the $Fe_2Co(\mu_3\text{-}O)$ cluster.[40] In the IR spectra of NH_2-MIL-88B(Fe_2Co), the characteristic peak at ~600 cm^{-1} which is responsible for the $Fe_2Co(\mu_3\text{-}O)$ core was disappeared along with the formation of two new bands (~600-700 cm^{-1}). This is because of the reduction of the site geometry from D_{3h} to C_{2v} during the substitution of metal ions which further lifts the asymmetric stretching vibration degeneracy for (metal-μ_3-O) core.[32, 41]

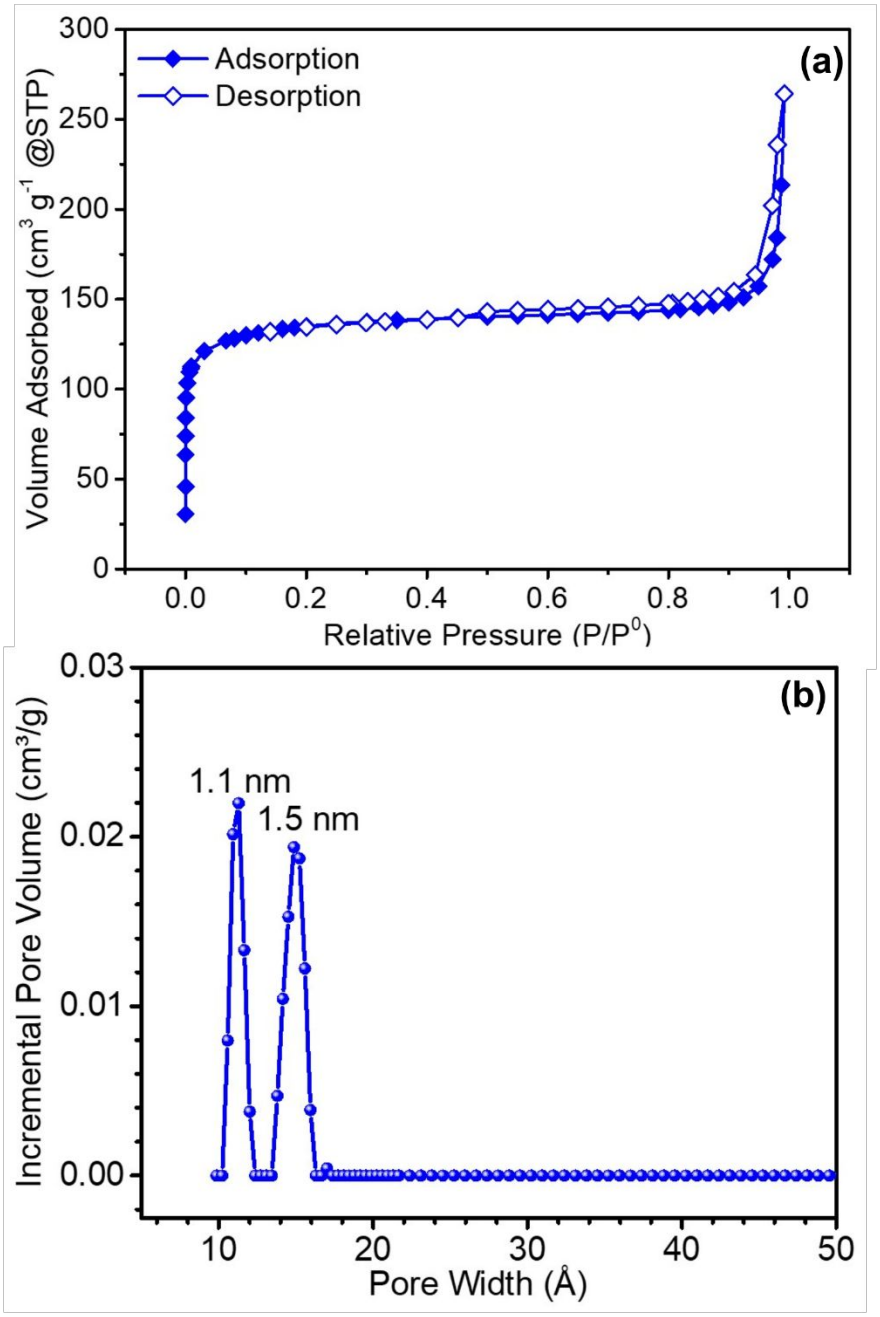

Figure 3. The N_2 gas adsorption/desorption isotherm curves of NH_2-MIL-88B(Fe_2Co) grown on NF. (b) The DFT pore size distribution curve for NH_2-MIL-88B(Fe_2Co) grown on NF.

Electrochemical measurements

In this study, the electrochemical studies were used to confirm the desired fabrication and functionalization of immunosensor. The electrochemical analyses using EIS and CV techniques

provide useful results to support the successful assembly of anti-cTnI tagged NH_2-MIL-88B(Fe_2Co)/NF electrodes and cTnI detection.

Electrochemical impedance spectroscopy

The EIS is a sensitive technique to identify the surface modifications in the field of biosensors that is especially used to detect the biomolecular interactions occurring at the interface between an electrode surface and electrolyte. The semicircle/straight line formations at high/low frequencies in the EIS typically represents the electron transfer/diffusion processes, respectively.[42] The results of EIS studies are presented as Nyquist plots obtained by plotting the imaginary (Z", out-of-phase) against the real (Z', in-phase) impedance components at various frequencies. The R_{ct} is measured from the EIS studies which indicate the real component of impedance. The impedance sensors are categorized into two types such as capacitive and faradaic based on the assessed signal nature. The capacitive current was measured in the absence of an electrolytic redox probe with a small sinusoidal voltage. Generally, the faradaic impedimetric sensors display enhanced sensitivity to the antibody-antigen binding. The electrode surface is covered with antibodies that can catalyze the redox probe to generate R_{ct} values. Moreover, the R_{ct} values tend to increase concerning antibody-antigen binding since the faradaic reaction gets increasingly hindered. The semicircle diameter obtained from the plot is used to compute the R_{ct} values. The low R_{ct} values directly indicate the fast electron transfer rate between electrodes used and electrolytes. [43-45] The R_{ct} values obtained from the impedance studies were extracted by fitting the data using Randle's equivalent circuit model.

The EIS measurements were recorded at different steps to confirm the bioconjugation of anti-cTnI-with the NH_2-MIL-88B(Fe_2Co)/NF electrode and subsequent antigen detection. The anti-cTnI- NH_2-MIL-88B(Fe_2Co)/NF electrode is shown exhibit low R_{ct} since the electrode surface

is readily accessible to the redox probe. The association of antigens to the electrode surface introduces an electrical contacting barrier for a redox label dissolved in a corresponding electrolytic solution which makes the electrode to receive high R_{ct} at the conducting support. The exposure of Ab-NH_2-MIL-88B(Fe_2Co)/NF immunosensor towards the targeted protein cTnI resulted in a further increase in R_{ct}, thus determining the potential affinity of the fabricated sensor towards cTnI. The enhancement in R_{ct} is due to the increased steric hindrance in the presence of antigens in addition to the electrolytic interactions between the electrolyte and analytes.

3D immunosensor fabrication

The fabrication and stepwise modification processes of the NF modified NH_2-MIL-88B(Fe_2Co)-MOF electrode was successfully measured using the impedance spectra based on the redox process of $[Fe(CN)_6]^{3-/4-}$ electrolyte and conventional Randle's circuit (**Figure S5**) and cyclic voltammetry. In this circuit, the ohmic resistance of an electrolytic solution is denoted as R_s; the charge transfer resistance is represented as R_{ct}. Once the NF was modified with NH_2-MIL-88B(Fe_2Co)-MOF, the R_{ct} is significantly reduced since NH_2-MIL-88B(Fe_2Co)-MOF catalyze the charge transfer process of the redox probe **(Figure S6)**. Further increase in the R_{ct} can be observed on the subsequent addition of antibody on the NH_2-MIL-88B(Fe_2Co)-MOF modified NF electrode. The functionalized electrodes were washed with Tween and treated with BSA. The increased R_{ct} values indicated that BSA was successively combined on the electrode surface to obstruct the processing electron process of the redox probe. The current form of the electrode is suitable to target cTnI. The electrode functionalization was also checked using cyclic voltammetry. The results shown in **Figure S7** are evident for the changes in the peak current further indicated the functionalization of the electrode with the antibody.

cTnI detection using 3D immunosensor

The Ab-NH_2-MIL-88B(Fe_2Co)-MOF/NF electrode was used to carry out the impedimetric analysis of cTnI in a concentration range of 1 ng/ml to 1 fg/ml in both assay buffer and 10 % serum conditions. The results were generated as Nyquist plots for the EIS measurements of different cTnI concentrations and are shown in **Figure 4.** Gradual enhancement in the semicircular diameter of the plot has been noticed with an enhanced cTnI concentration. The interactions between antibody and antigens at the electroactive surface altered the dielectric layer properties and block the charge transport over the electrode surface and redox probe. Since the Faradaic reaction was restricted, the R_{ct} values increased linearly to the cTnI concentration and confirm the binding affinity of antibody-antigens. The LOD of the anti-cTnI tagged NH_2-MIL-88B(Fe_2Co)/NF immunosensor was calculated as 13 fg/ml which is lower than the reported normal range (0.1-0.4 ng/ml)[46] and the value obtained is better than those of previous EIS reports (**Table 1**).

The practical application of anti-cTnI tagged NH_2-MIL-88B(Fe_2Co)/NF immunosensor was tested by conducting the analyses in 10% serum solutions. In this analysis, serum samples were spiked with known cTnI antigens and subjected to EIS analyses to record their corresponding R_{ct} values. The result of this analysis is shown in **Figures 4c** and **4d.** The acceptable recoveries (98-107%)[36, 47] of the spiked up antigens were obtained, thus demonstrating that the fabricated sensor could be used for the potential analysis of cTnI even in real samples. The LOD was also achieved quite similar to that obtained for pure antigens. It can be concluded from this experimental result that anti-cTnI tagged NH_2-MIL-88B(Fe_2Co)/NF immunosensor can be used as an effective tool for the detection of cTnI.

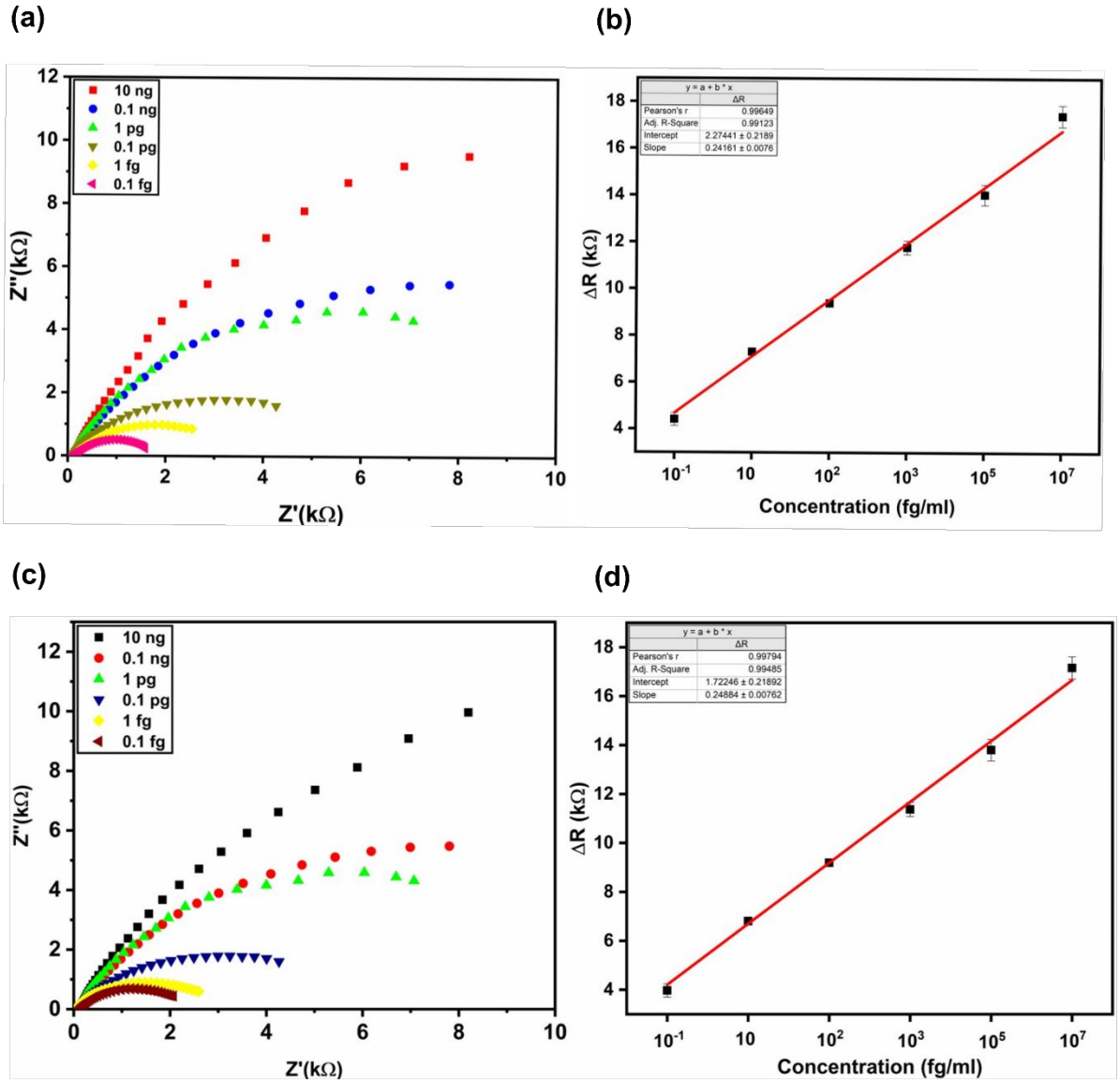

Figure 4. Nyquist plots obtained from EIS measurements during the analysis of various cTnI concentrations (0.1 fg/ml – 10 ng/ml) using an equimolar mixture of $[Fe(CN)_6]^{3-/4-}$ as a redox probe. (a) Concentration dependent study in buffer solution. (b) The plot of concentration versus R_{ct} recorded for (a). (c) Concentration dependent study in serum solution. (d) The plot of concentration versus R_{ct} recorded for (c).

Table 1. Recent studies on the analytical performance of the electrode for cTnI detection based on EIS.

Platform	**Linear range (ml^{-1})**	**LOD/LOQ (ml^{-1})**	**References**
Ab-cTnI-AgMPA-APTES-ITO	20 ng-1 µg	5.5 ng	[48]
Mn_3O_4-RGO	0.008-20 ng	8.0 pg	[49]
Graphene oxide-gold nanoparticles	1-1400 ng	0.67 ng	[50]
GQDs-Antibody	0.01-100 ng	0.01 ng	[51]
Cd ion nanocrystal-MOF	0.1-20 ng	0.1 ng	[52]
Porous graphene oxide	0.1-10 ng	0.07 ng	[53]
ZnO based electrode	-	1 pg	[54]
Ab-NH_2-MIL-88B(Fe_2Co)-MOF/NF	10 ng-0.1 fg	13 fg	Present work

Cyclic voltammetry

The I-V characteristics of the Ab-NH_2-MIL-88B(Fe_2Co)-MOF electrode towards cTnI detection were measured using cyclic voltammetry. The Ab-NH_2-MIL-88B(Fe_2Co) electrode was used for the immunoassay of various concentrations of cTnI (0.1 fg/ml – 100 ng/ml). An aliquot of 10 µl of cTnI was dropped on the Ab-NH_2-MIL-88B(Fe_2Co)-MOF electrode surface and the recorded each measurement after 10 min. Before each measurement, the electrodes were cleaned with PBS and water to remove any unbound proteins. The interaction between antigen and antibody results in net electrical charge of Ab-NH_2-MIL-88B(Fe_2Co) electrode which further led to a change in overall conductance of the fabricated immunosensor. The results of I-V data for different cTnI concentrations (0.1 fg/ml -100 ng/ml) are given in **Figure S8**. It is found that the conductance of the Ab-NH_2-MIL-88B(Fe_2Co)-MOF electrode was found to decrease when

exposed to high protein concentrations. The surface modification results in the reduction of peak current intensity as the biomolecules obstruct the charge transfer process redox probe.

Selectivity and reproducibility

The specificity of 3D immunosensor, Ab-NH_2-MIL-88B(Fe_2Co)-MOF/NF in the presence of non-specific BSA (1 mg/ml) was evaluated as a control experiment **(Figure S9)**. Then the selectivity of the Ab-NH_2-MIL-88B(Fe_2Co)/NF electrode was checked by conducting the EIS experiments with avidin, FSH, and cTnT **(Figure 5a)**.

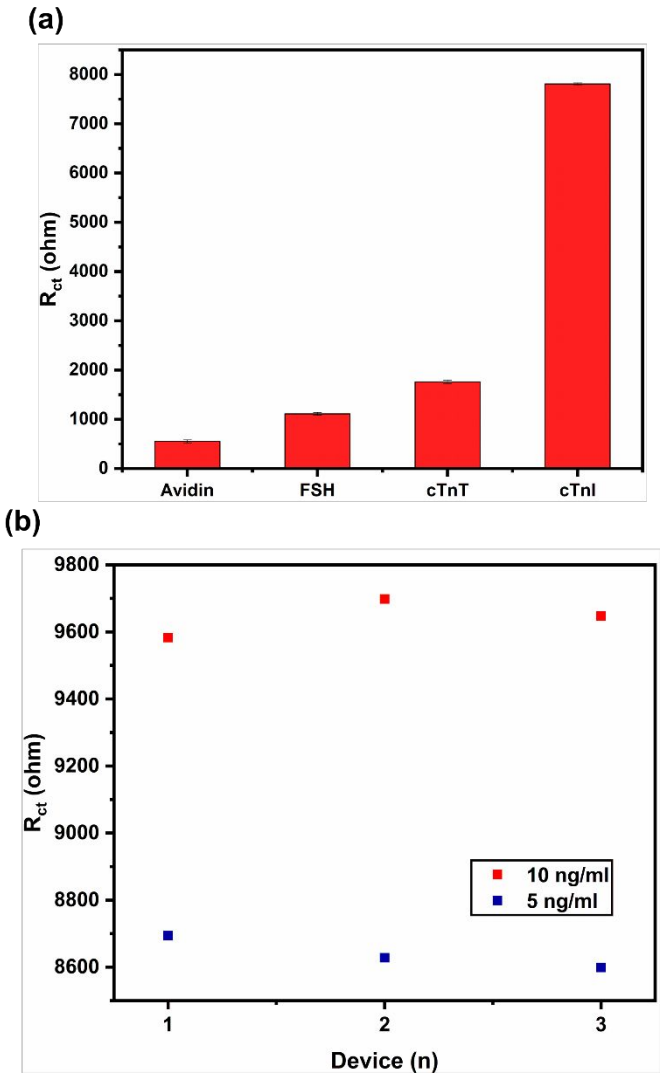

Figure 5. (a) Selectivity of Ab-NH_2-MIL-88B(Fe_2Co)/NF towards avidin (10 μg/ml), FSH (10 μg/ml), cTnT (10 μg/ml), and cTnI (10 μg/ml). (b) The EIS response of a two sensor chips obtained from three different batches to detect three different cTnI concentrations (5 ng/ml and 10 ng/ml).

The specificity results obtained indicate that the charge transfer resistance of the 3D immunosensor towards cTnI detection showed an insignificant difference in the presence of non-specific proteins demonstrating its high specificity. The reproducibility of the 3D immunosensor is an essential parameter for practical studies. Hence, the devices fabricated from the three different batches were tested in detecting two different cTnI concentrations (5 ng/ml and 10 ng/ml) and the corresponding charge transfer resistance values were measured (**Figure 5b**). All the electrodes were made using different batch NH_2-MIL-88B(Fe_2Co) material and the R_{ct} values were measured under identical experimental conditions. These results indicated that R_{ct} values obtained from different batch electrodes displayed a closely similar response, successively showing the good reproducibility of the devices for cTnI detection.

Conclusions

In this study, a label-free, bimetallic in situ grown 3D nickel foam supported impedimetric immunosensor Ab-NH_2-MIL-88B(Fe_2Co)-MOF was fabricated. Selective and rapid detection of cTnI was achieved based on impedimetric monitoring of the antigen with covalently immobilized antibodies on the NF substrate both in buffer and serum solutions with LOD of 13 fg/ml. The immunosensor displayed greater specificity and this technique could be a potential alternative for monitoring cTnI when compared to traditional methods.

Supporting Information

Some of the additional data including SEM images, TEM image, FT-IR, equivalent circuit model, EIS measurements, CV measurements are provided in supporting information. SEM image and SEM-EDX of NH_2-MIL 88B(Fe_2Co)-MOF/NF (Figure S1); SEM image and the area SEM-EDX elemental mapping of NH_2-MIL-88B(Fe_2Co)-MOF/NF (Figure S2); TEM image and TEM-EDX elemental mapping of NH_2-MIL-88B(Fe_2Co)-MOF/NF (Figure S3); FT-IR spectra of $Fe_2Co(\mu_3\text{-}O)(CH_3COO)_6(H_2O)_3Fe_2CoO$ cluster and NH_2-MIL-88B(Fe_2Co)-MOF/NF (Figure S4); Equivalent circuit model (Figure S5); Electrochemical measurements for nickel foam (NF) modified MOF electrode (Figure S6); Cyclic voltammograms obtained during surface functionalization of the electrode (Figure S7); Cyclic voltammograms obtained during the cyclic voltammetry analysis of varying concentrations of cTnI (Figure S8); Specificity of the MOF electrode in the presence of non-specific BSA (Figure S9).

Conflicts of interest

There are no conflicts to declare.

Acknowledgements

We are grateful to the Ministry of Science and Technology, Taiwan, R.O.C. for financial support under MOST 108-2113-M-009-008. This work was financially supported by the "Center for Intelligent Drug Systems and Smart Bio-devices (IDS^2B)" from The Featured Areas Research Center Program within the framework of the Higher Education Sprout Project by the Ministry of Education (MOE) in Taiwan. This research is supported partially by Kaohsiung Medical University Research Center Grant (KMU-TC108A04-0).

References

(1) Altintas, Z.; Fakanya, W. M.; Tothill, I. E. Cardiovascular Disease Detection Using Bio-Sensing Techniques. Talanta 2014, 128, 177-186.
(2) Bhatnagar, D.; Kaur, I.; Kumar, A. Ultrasensitive Cardiac Troponin I Antibody Based Nanohybrid Sensor For Rapid Detection Of Human Heart Attack. Int. J. Biol. Macromol. 2017, 95, 505-510.
(3) Vasan, R. S. Biomarkers Of Cardiovascular Disease: Molecular Basis And Practical Considerations. Circulation 2006, 113 (19), 2335-2362.
(4) Tuteja, S. K.; Kukkar, M.; Suri, C. R.; Paul, A. K.; Deep, A. One Step In-Situ Synthesis Of Amine Functionalized Graphene For Immunosensing Of Cardiac Marker cTnI. Biosens. Bioelectron. 2015, 66, 129-135.
(5) Lim, W.; Qushmaq, I.; Devereaux, P. J.; Heels-Ansdell, D.; Lauzier, F.; Ismaila, A. S.; Crowther, M. A.; Cook, D. J. Elevated Cardiac Troponin Measurements in Critically Ill Patients. JAMA Int. Med. 2006, 166 (22), 2446-2454.
(6) Kim, K.; Park, C.; Kwon, D.; Kim, D.; Meyyappan, M.; Jeon, S.; Lee, J. S. Silicon Nanowire Biosensors For Detection Of Cardiac Troponin I (cTnI) With High Sensitivity. Biosens. Bioelectron. 2016, 77, 695-701.
(7) Zhou, Y.; Zhuo, Y.; Liao, N.; Chai, Y.; Yuan, R. Ultrasensitive Electrochemiluminescent Detection Of Cardiac Troponin I Based On A Self-Enhanced Ru(II) Complex. Talanta 2014, 129, 219-226.
(8) Kar, P.; Pandey, A.; Greer, J. J.; Shankar, K. Ultrahigh Sensitivity Assays For Human Cardiac Troponin I Using TiO2 Nanotube Arrays. Lab on a chip 2012, 12 (4), 821-828.
(9) Dempsey, E.; Rathod, D. Disposable Printed Lateral Flow Electrochemical Immunosensors for Human Cardiac Troponin T. IEEE Sens. J. 2018, 18 (5), 1828-1834.
(10) Elgqvist, J. Nanoparticles As Theranostic Vehicles In Experimental And Clinical Applications-Focus On Prostate And Breast Cancer. Int. J. Mol. Sci. 2017, 18 (5), pii: E1102.
(11) Foubert, A.; Beloglazova, N. V.; Hedstrom, M.; De Saeger, S. Antibody Immobilization Strategy For The Development Of A Capacitive Immunosensor Detecting Zearalenone. Talanta 2019, 191, 202-208.
(12) Sayikli Simsek, C.; Nur Sonuc Karaboga, M.; Sezginturk, M. K. A New Immobilization Procedure For Development Of An Electrochemical Immunosensor For Parathyroid Hormone Detection Based On Gold Electrodes Modified With 6-Mercaptohexanol And Silane. Talanta 2015, 144, 210-218.
(13) Shoute, L. C. T.; Anwar, A.; MacKay, S.; Abdelrasoul, G. N.; Lin, D.; Yan, Z.; Nguyen, A. H.; McDermott, M. T.; Shah, M. A.; Yang, J.; Chen, J.; Li, X. S. Immuno-Impedimetric Biosensor For Onsite Monitoring Of Ascospores And Forecasting Of Sclerotinia Stem Rot Of Canola. Sci. Rep. 2018, 8 (1), 12396-12396.
(14) Spain, E.; Gilgunn, S.; Sharma, S.; Adamson, K.; Carthy, E.; O'Kennedy, R.; Forster, R. J. Detection Of Prostate Specific Antigen Based On Electrocatalytic Platinum Nanoparticles Conjugated To A Recombinant Scfv Antibody. Biosens. Bioelectron. 2016, 77, 759-766.
(15) Suni, I. I. Impedance Methods For Electrochemical Sensors Using Nanomaterials. TrAC Trend. Anal. Chem. 2008, 27 (7), 604-611.

(16) Alkordi, M. H.; Liu, Y.; Larsen, R. W.; Eubank, J. F.; Eddaoudi, M. Zeolite-Like Metal−Organic Frameworks As Platforms For Applications: On Metalloporphyrin-Based Catalysts. J. Am. Chem. Soc. 2008, 130 (38), 12639-12641.
(17) Chen, Q.; Zhang, X.; Li, S.; Tan, J.; Xu, C.; Huang, Y. MOF-derived Co_3O_4@Co-Fe Oxide Double-Shelled Nanocages As Multi-Functional Specific Peroxidase-Like Nanozyme Catalysts For Chemo/Biosensing And Dye Degradation. Chem. Eng. J. 2020, 8 (13), 1703242.
(18) Furukawa, H.; Cordova, K. E.; O'Keeffe, M.; Yaghi, O. M. The Chemistry And Applications Of Metal-Organic Frameworks. Science 2013, 341 (6149), 1230444.
(19) Guo, Y.; Feng, X.; Han, T.; Wang, S.; Lin, Z.; Dong, Y.; Wang, B. Tuning The Luminescence Of Metal–Organic Frameworks For Detection Of Energetic Heterocyclic Compounds. J. Am. Chem. Soc. 2014, 136 (44), 15485-15488.
(20) Kundu, T.; Mitra, S.; Patra, P.; Goswami, A.; Diaz Diaz, D.; Banerjee, R. Mechanical Downsizing Of A Gadolinium(III)-Based Metal-Organic Framework For Anticancer Drug Delivery. Chemistry 2014, 20 (33), 10514-10518.
(21) Li, S.; Hou, Y.; Chen, Q.; Zhang, X.; Cao, H.; Huang, Y. Promoting Active Sites In MOF-Derived Homobimetallic Hollow Nanocages As A High-Performance Multifunctional Nanozyme Catalyst For Biosensing And Organic Pollutant Degradation. ACS Appl. Mater. Interfaces 2020, 12 (2), 2581-2590.
(22) Wu, F.; Zhang, S.; Xi, B.; Feng, Z.; Sun, D.; Ma, X.; Zhang, J.; Feng, J.; Xiong, S. Unusual Formation Of CoO@C “Dandelions” Derived From 2D Kagóme MOLs For Efficient Lithium Storage. Adv. Funct. Mater. 2018, 8 (13), 1703242.
(23) Yang, L.; Zeng, X.; Wang, W.; Cao, D. Recent Progress in MOF-Derived, Heteroatom-Doped Porous Carbons As Highly Efficient Electrocatalysts For Oxygen Reduction Reaction In Fuel Cells. Adv. Funct. Mater. 2018, 28 (7), 1704537.
(24) Zhang, M.; Dai, Q.; Zheng, H.; Chen, M.; Dai, L. Novel MOF-Derived Co@N-C Bifunctional Catalysts For Highly Efficient Zn–Air Batteries And Water Splitting. Adv. Mater. 2018, 30 (10), 1705431.
(25) Zhang, L.; Ye, C.; Li, X.; Ding, Y.; Liang, H.; Zhao, G.; Wang, Y. A CuNi/C Nanosheet Array Based On A Metal–Organic Framework Derivate As A Supersensitive Non-Enzymatic Glucose Sensor. Nano-micro Lett. 2017, 10 (2), 28.
(26) Torrisi, A.; Bell, R. G.; Mellot-Draznieks, C. Predicting The Impact Of Functionalized Ligands On CO2 Adsorption In Mofs: A Combined DFT And Grand Canonical Monte Carlo Study. Micropor. Mesopor. Mater. 2013, 168, 225-238.
(27) Xiong, G.; Qin, X. Y.; Shi, P. F.; Hou, Y. L.; Cui, J. Z.; Zhao, B. New Strategy To Construct Single-Ion Magnets: A Unique Dy@Zn(6) Cluster Exhibiting Slow Magnetic Relaxation. Chem. Commun. 2014, 50 (32), 4255-4257.
(28) Chaudhari, N. K.; Jin, H.; Kim, B.; Lee, K. Nanostructured Materials On 3D Nickel Foam As Electrocatalysts For Water Splitting. Nanoscale 2017, 9 (34), 12231-12247.
(29) Luo, J.; Im, J. H.; Mayer, M. T.; Schreier, M.; Nazeeruddin, M. K.; Park, N. G.; Tilley, S. D.; Fan, H. J.; Gratzel, M. Water Photolysis At 12.3% Efficiency Via Perovskite Photovoltaics And Earth-Abundant Catalysts. Science 2014, 345 (6204), 1593-1596.
(30) Lu, B.; Cao, D.; Wang, P.; Wang, G.; Gao, Y. Oxygen Evolution Reaction On Ni-Substituted Co3O4 Nanowire Array Electrodes. Int. J. Hydrog. 2011, 36 (1), 72-78.
(31) Taylor, J. M.; Dawson, K. W.; Shimizu, G. K. H. A Water-Stable Metal–Organic Framework With Highly Acidic Pores For Proton-Conducting Applications. J. Am. Chem. Soc. 2013, 135 (4), 1193-1196.

(32) Peng, L.; Asgari, M.; Mieville, P.; Schouwink, P.; Bulut, S.; Sun, D. T.; Zhou, Z.; Pattison, P.; van Beek, W.; Queen, W. L. Using Predefined M3(μ3-O) Clusters As Building Blocks For An Isostructural Series Of Metal–Organic Frameworks. ACS Appl. Mater. Interfaces 2017, 9 (28), 23957-23966.
(33) Senthil Raja, D.; Chuah, X.-F.; Lu, S.-Y. In Situ Grown Bimetallic MOF-Based Composite As Highly Efficient Bifunctional Electrocatalyst For Overall Water Splitting With Ultrastability At High Current Densities. Adv. Energy Mat. 2018, 8 (23), 1801065.
(34) Senthil Raja, D.; Lin, H.-W.; Lu, S.-Y. Synergistically Well-Mixed Mofs Grown On Nickel Foam As Highly Efficient Durable Bifunctional Electrocatalysts For Overall Water Splitting At High Current Densities. Nano Energy 2019, 57, 1-13.
(35) Song, Y.; Qiang, T.; Ye, M.; Ma, Q.; Fang, Z. Metal Organic Framework Derived Magnetically Separable 3-Dimensional Hierarchical Ni@C Nanocomposites: Synthesis And Adsorption Properties. Appl. Surf. Sci. 2015, 359, 834-840.
(36) Tuteja, S. K.; Chen, R.; Kukkar, M.; Song, C. K.; Mutreja, R.; Singh, S.; Paul, A. K.; Lee, H.; Kim, K.-H.; Deep, A.; Suri, C. R. A Label-Free Electrochemical Immunosensor For The Detection Of Cardiac Marker Using Graphene Quantum Dots (GQDs). Biosens. Bioelectron. 2016, 86, 548-556.
(37) Dong, H.; Zhang, X.; Yan, X. C.; Wang, Y. X.; Sun, X.; Zhang, G.; Feng, Y.; Zhang, F. M. Mixed-Metal-Cluster Strategy For Boosting Electrocatalytic Oxygen Evolution Reaction Of Robust Metal-Organic Frameworks. ACS Appl. Mater. Interfaces 2019, 11 (48), 45080-45086.
(38) Zhao, X.; Pattengale, B.; Fan, D.; Zou, Z.; Zhao, Y.; Du, J.; Huang, J.; Xu, C. Mixed-Node Metal–Organic Frameworks As Efficient Electrocatalysts For Oxygen Evolution Reaction. ACS Energy Lett. 2018, 3 (10), 2520-2526.
(39) Serre, C.; Mellot-Draznieks, C.; Surble, S.; Audebrand, N.; Filinchuk, Y.; Ferey, G. Role Of Solvent-Host Interactions That Lead To Very Large Swelling Of Hybrid Frameworks. Science 2007, 315 (5820), 1828-1831.
(40) Shova, S. G.; Cadelnic, I. G.; Gdaniec, M.; Simonov, Y. A.; Jovmir, T. C.; Meriacre, V. M.; Filoti, G.; Turta, C. I. Syntheses And Structural Study Of Trinuclear Iron Acetates $[Fe_3O(CH_3COO)_6(H_2O)_3]Cl\cdot 6H_2O$ And $[Fe_3O(CH_3COO)_6(H_2O)_3]\,[FeCl_4]\cdot 2CH_3COOH$. J. Struc. Chem. 1998, 39 (5), 747-761.
(41) Yazdanbakhsh, M.; Lotfian, N.; Tavakkoli, H.; Boese, R. Synthesis, Characterization And Crystal Structure Analysis Of A Novel Oxo-Centered Mixed-Metal Complex Containing Unsaturated Bridging Carboxylates. Cent. Eur. J. Chem. 2011, 9, 585-589.
(42) Huang, K.-J.; Niu, D.-J.; Sun, J.-Y.; Han, C.-H.; Wu, Z.-W.; Li, Y.-L.; Xiong, X.-Q. Novel Electrochemical Sensor Based On Functionalized Graphene For Simultaneous Determination Of Adenine And Guanine In DNA. Colloids Surf. B Biointerfaces 2011, 82 (2), 543-549.
(43) Alfonta, L.; Bardea, A.; Khersonsky, O.; Katz, E.; Willner, I. Chronopotentiometry And Faradaic Impedance Spectroscopy As Signal Transduction Methods For The Biocatalytic Precipitation Of An Insoluble Product On Electrode Supports: Routes For Enzyme Sensors, Immunosensors And DNA Sensors. Biosens. Bioelectron. 2001, 16 (9-12), 675-687.
(44) Bardea, A.; Katz, E.; Willner, I. Probing Antigen–Antibody Interactions On Electrode Supports By The Biocatalyzed Precipitation Of An Insoluble Product. Electroanalysis 2000, 12 (14), 1097-1106.
(45) Pei, R.; Cheng, Z.; Wang, E.; Yang, X. Amplification Of Antigen-Antibody Interactions Based On Biotin Labeled Protein-Streptavidin Network Complex Using Impedance Spectroscopy. Biosens. Bioelectron. 2001, 16 (6), 355-361.

(46) Fuchs, S.; Kornowski, R.; Mehran, R.; Satler, L. F.; Pichard, A. D.; Kent, K. M.; Hong, M. K.; Slack, S.; Stone, G. W.; Leon, M. B. Cardiac Troponin I Levels And Clinical Outcomes In Patients With Acute Coronary Syndromes: The Potential Role Of Early Percutaneous Revascularization. J. Am. Coll. Cardiol. 1999, 34 (6), 1704-1710.
(47) Wang, M.; Liu, J.; Qin, X.; Nie, X.; Dong, Y.; Liang, X.; Zhu, Z.; Yang, D.; Shao, Y. Electrochemiluminescence Detection Of Cardiac Troponin I Based On Au–Ag Alloy Nanourchins. Analyst 2020, 145 (3), 873-879.
(48) Xiong, M.; Wang, X.; Kong, Y.; Han, B. Development Of Cardiac Troponin I Electrochemical Impedance Immunosensor. Int. J. Electrochem. Sci. 2017, 12, 4204-4214.
(49) Singh, N.; Ali, M. A.; Rai, P.; Sharma, A.; Malhotra, B. D.; John, R. Microporous Nanocomposite Enabled Microfluidic Biochip For Cardiac Biomarker Detection. ACS Appl. Mater. Interfaces 2017, 9 (39), 33576-33588.
(50) Singh, S.; Tuteja, S. K.; Sillu, D.; Deep, A.; Suri, C. R. Gold Nanoparticles-Reduced Graphene Oxide Based Electrochemical Immunosensor For The Cardiac Biomarker Myoglobin. Microchim. Acta 2016, 183 (5), 1729-1738.
(51) Tuteja, S. K.; Chen, R.; Kukkar, M.; Song, C. K.; Mutreja, R.; Singh, S.; Paul, A. K.; Lee, H.; Kim, K. H.; Deep, A.; Suri, C. R. A Label-Free Electrochemical Immunosensor For The Detection Of Cardiac Marker Using Graphene Quantum Dots (GQDs). Biosens. Bioelectron. 2016, 86, 548-556.
(52) Deep, A.; Bhardwaj, S. K.; Paul, A. K.; Kim, K.-H.; Kumar, P. S Surface Assembly Of Nano-Metal Organic Framework On Amine Functionalized Indium Tin Oxide Substrate For Impedimetric Sensing Of Parathion. Biosens. Bioelectron. 2015, 65, 226-231.
(53) Kazemi, S. H.; Ghodsi, E.; Abdollahi, S.; Nadri, S. Porous Graphene Oxide Nanostructure As An Excellent Scaffold For Label-Free Electrochemical Biosensor: Detection Of Cardiac Troponin I. Mat. Sci. Eng. C-Mater. 2016, 69, 447-452.
(54) Radha Shanmugam, N.; Muthukumar, S.; Chaudhry, S.; Anguiano, J.; Prasad, S. Ultrasensitive Nanostructure Sensor Arrays On Flexible Substrates For Multiplexed And Simultaneous Electrochemical Detection Of A Panel Of Cardiac Biomarkers. Biosens. Bioelectron. 2017, 89, 764-772.

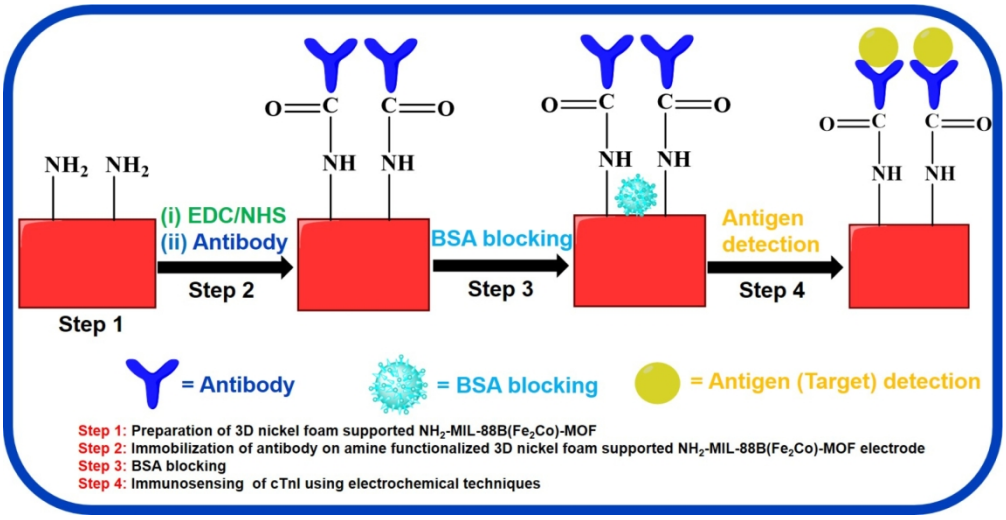
NH2 NH2
(i) EDC/NHS
(ii) Antibody
Step 2
BSA blocking
Step 3
Antigen detection
Step 4
Step 1
= Antibody
= BSA blocking
= Antigen (Target) detection
Step 1: Preparation of 3D nickel foam supported NH2-MIL-88B(Fe2Co)-MOF
Step 2: Immobilization of antibody on amine functionalized 3D nickel foam supported NH2-MIL-88B(Fe2Co)-MOF electrode
Step 3: BSA blocking
Step 4: Immunosensing of cTnI using electrochemical techniques